

Tunneling probe-based identification of the sp^3 dangling bond on the H–C(100):2 × 1 surface

Lachlan Oberg^{1,2}, Yi-Ying Sung³, Cedric Weber⁴, Marcus W. Doherty⁴, and Christopher I. Pakes³

¹ Department of Quantum Science and Technology, Research School of Physics, Australian National University, Canberra 2601, Australia.

² School of Civil & Environmental Engineering, Faculty of Engineering, Queensland University of Technology, Gardens Point Campus, Brisbane, QLD 4000, Australia.

³ Department of Mathematical and Physical Sciences, La Trobe University, Victoria 3086, Australia. and

⁴ Quantum Brilliance Pty Ltd, 60 Mills Road, Acton, ACT 2601, Australia.

(Dated: January 30, 2026)

The sp^3 dangling bond on the diamond surface plays a critical role in the performance and fabrication of diamond quantum technologies. For the former, the magnetic and electric properties of this defect can impede the performance of quantum sensors and computers. For the latter, the chemical properties of the dangling bond are integral to proposed methods for bottom-up fabrication of scalable diamond quantum devices. In pursuit of high performance and scalable diamond quantum technology, tunneling probe-based techniques offers the ability to create and modify the sp^3 dangling bond with atomic-scale precision. However, these capabilities cannot be realised either deterministically or at scale without a means for identifying the sp^3 dangling bond amidst the myriad of other defects on the diamond surface. Consequently, in this work we provide a comprehensive experimental and theoretical framework for STS-based characterisation of the sp^3 defect on the H-terminated (100) diamond surface. This capability provides the foundation for future tunneling probe studies in the modification of dangling bonds.

I. INTRODUCTION

The sp^3 dangling bond on the hydrogen-terminated diamond surface has immense significance for diamond quantum technologies. As depicted in Figure 1, this defect is formed through the desorption of a terminating H atom and is a common byproduct during diamond chemical vapor deposition (CVD) growth and surface preparation[1–3]. On the technologically important (100) and (111) surfaces, the defect possesses an unsatisfied electron at the bare carbon (C) surface site with an sp^3 bond hybridisation. Unfortunately, it exhibits paramagnetic and charge trapping behaviour which can impede the performance of diamond quantum computers and quantum sensors which rely upon near-surface nitrogen-vacancy (NV) centres[2–7]. This is chiefly through the production of magnetic and electric noise which reduce NV coherence times and cause electric field screening during electrometry.

Fortunately, recent results have demonstrated that the deleterious effects of the sp^3 dangling bond can be neutralised through H capping[3]. Voltage pulses are applied to a hydrogen-functionalised scanning tunneling microscope (STM) tip to passivate individual defects with H termination. However, this capping procedure is currently unreliable, with poor control, yield, and a spatial resolution on the order of nanometres. Moreover, due to visual similarities with other benign surface defects, identifying sp^3 dangling bonds for H capping can be challenging. While the defects may be differentiated using high-resolution STM imaging, scanning tunneling spectroscopy (STS) offers an alternative and direct means for identifying sp^3 dangling bonds, but has not been sub-

stantively explored in the literature.

Additionally, recent work has proposed that scalable diamond quantum devices could be fabricated through the targeted creation of sp^3 dangling bonds[8–11]. Termed H desorption lithography (HDL), this process involves applying voltage pulses to an STM tip for the targeted removal of H termination[12]. This produces reactive clusters of dangling bonds which subsequently act as active sites for chemical adsorption of a N-based gas. Lastly, the surface is overgrown using CVD to produce bulk NV centres. By using HDL to produce many active sites simultaneously, it may be possible to realise a large-scale diamond quantum device containing many coupled NV centres. However, a key requirement for this multi-step process is validating the production of dangling bonds following lithography. This analysis could be greatly enhanced through STS, which provides a distinct signature that reveals the energetic structure of the sp^3 dangling bond.

Consequently, the aim of this work is to characterise the STS spectra of sp^3 dangling bonds through a combined theoretical and experimental approach. While first-principles calculations have previously determined the defect electronic structure[3], this structure has yet to be aligned with features of experimental STS (of which there are limited examples in the literature). Furthermore, performing this alignment is greatly complicated due to band bending on diamond surfaces. Diamond STM/STS typically relies on boron doping to achieve relatively low conductivities under UHV conditions. Electric fields are therefore poorly screened at the diamond surface resulting in significant band bending[3]. In contrast to STM/STS on metallic surfaces, the applied bias

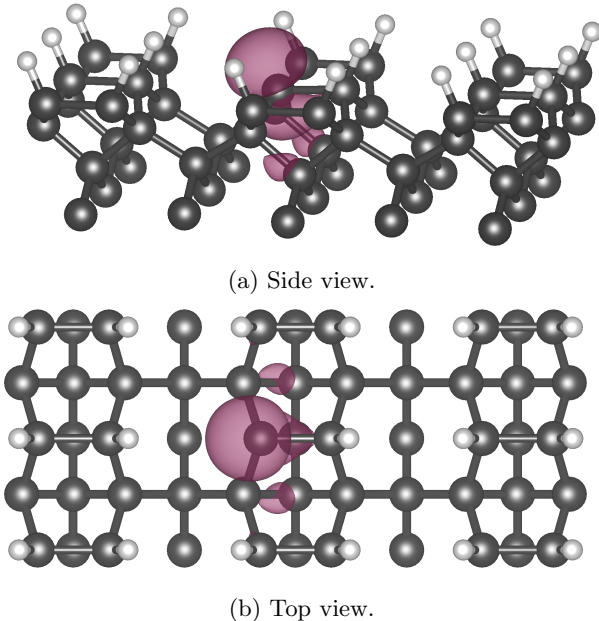


FIG. 1: Atomic structure of the sp^3 dangling bond on the H-C(100): 2×1 surface. Hydrogen ions are white and carbon atoms are grey. A single hydrogen ion has been removed from the dimerised surface, exposing a bare surface carbon with an sp^3 dangling bond. This dangling bond produces localised states within the diamond band gap which can be visualised using STM. Depicted in purple is the charge density corresponding to an unoccupied mid-gap state.

between tip and sample is *not* commensurate to the energetic translation of the tip Fermi level relative to surface states. Hence, peak positions in STS spectra are not necessarily equivalent to the energy of surface electronic states[13, 14]. Careful analysis is therefore required to account for modifications in STS spectra due to band bending.

The outline of this work is as follows. In section II we present our experimental and theoretical methodology. This entails STS of an sp^3 dangling bond occurring on an as-grown H-C(100): 2×1 surface, calculating the defect electronic structure using density functional theory, and modeling the effects of band bending using electrostatic simulations. Section III presents the resulting experimental spectrum, theoretical band structure, and surface band bending. In Section IV we synthesise these results to assign peaks in the experimental spectrum with electronic states of the defect. Moreover, this assignment process enables calculation of the acceptor concentration and absolute tip-surface distance. The former introduces STS as a bulk characterisation tool whereas the latter is a long-standing challenge in STM. Finally, Section V concludes that STS in combination with STM imaging provides a viable means for identifying sp^3 dangling bonds.

II. METHODOLOGY

A. Experimental

STM and STS were carried out using a SPECS Aarhus UHV-STM operating at room temperature and under ultra-high vacuum (UHV) with a base pressure of 10^{-9} mbar. CVD-grown C(100) samples of dimensions 3.5×3.5 mm 2 were outgassed at 823 K for 1 h to remove airborne surface impurities and produce a small number of dangling bonds. STM images were recorded in constant current mode at +2.5 V sample bias (i.e., imaging the empty states) and with the tunnelling current set to 0.3 nA. dI/dV single point spectra were obtained by positioning the STM tip on either the dimer row or the dangling bond sites. The spectra were recorded using a lock-in amplifier (modulated at 583 Hz with 50 mV peak-to-peak amplitude) while ramping the sample bias from +4 V (or +2.0 V) to -2.5 V at constant tip-sample distance. This fixed distance corresponded to tunnelling conditions at $I = 0.30$ nA and $V = 4$ V.

B. Density functional theory

Density functional theory was performed using the *Vienna ab initio software package* (VASP)[15–17]. The H-C(100): 2×1 surface and sp^3 dangling bond was represented using a 419-ion slab with a thickness of 8 carbon layers and lateral dimensions of 17.7 Å \times 15.2 Å. The slab geometry was optimised using PBE[18] calculations to a force tolerance of 5×10^{-3} eV/Å per ion. We use a plane-wave cut-off of 600 eV, a $4 \times 4 \times 1$ Γ -centered k -point mesh, and the total energy was optimised to 10^{-4} eV. Using the optimised slab geometry, we then perform Γ -point calculations using the HSE06 functionals[19] and a constant electric field (treated self-consistently) between ± 0.2 V/Å. Details of the slab model can be found in [3].

C. Electrostatic modeling

The effects of band bending during diamond STS were simulated through electrostatic modeling with COMSOL Multiphysics. Poisson's equation was solved via finite element analysis for a space-charge density and geometry appropriate for a metallic tip above the surface of boron-doped diamond. Extensive details regarding this modeling are provided in [3] and [9]. Simulations were performed for range of tip-sample separation distances and boron concentrations. The key results of this modeling are the voltage drop (V_d , defined as the voltage difference between the tip and sample surface) and electric field at the diamond surface at the position directly beneath the tip apex. These two values define all aspects of band bending needed to interpret the STS spectra, and were calculated as a function of applied bias (V_a) between the tip and sample backplate.

III. RESULTS

A. Experimental STS

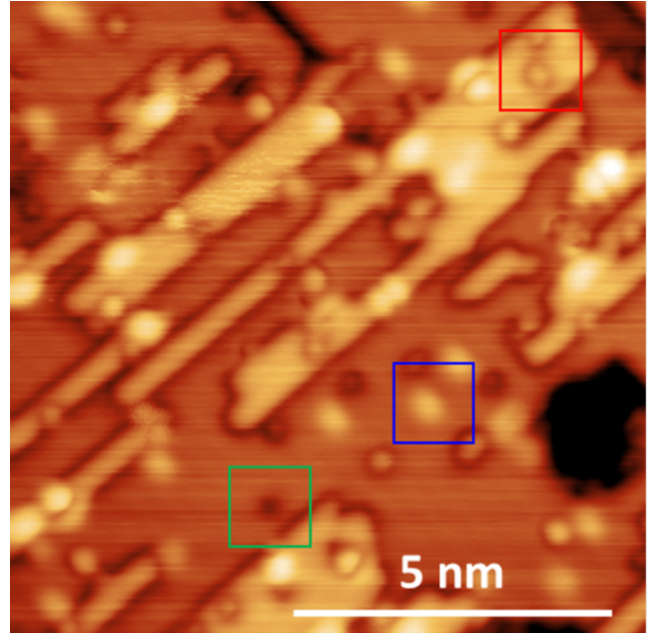
High-resolution STM imaging was first used to identify an sp^3 dangling bond on the H-C(100):2 \times 1 surface. A constant current topography of the diamond surface after annealing at 823 K for an hour is presented in Figure 2 (a). Different defects can be observed on the surface and identified based on the symmetry of their STM topographies[3]. The sp^3 dangling bond is highlighted in blue and is characterised by a bright, chestnut-shaped feature. This identification was confirmed post STS by re-passivating the dangling bond through a targeted voltage sweep. Known as hydrogen ‘capping’, this technique is an additional means to identify dangling bonds as documented by Sung *et al*[3].

The electronic structure of this particular sp^3 dangling bond was then studied using STS. It was chosen due to its isolation from other defects and step edges which could interfere with its electronic properties or lead to unwanted tunnelling. A single-point dI/dV spectra was acquired on the sp^3 dangling bond over a voltage range between -2.5 V and $+4$ V (sample bias). The spectrum is presented in Figure 2 (b). Two distinct peaks are present and centered at -2.1 V and $+3.4$ V. These peaks are not associated with the underlying electronic structure of the H-C(100):2 \times 1 surface as they do not appear in the STS spectrum on the reconstructed dimer rows. Consequently, the two peaks are produced by tunneling into defect electronic states and will therefore form the basis of our investigation in Section IV.

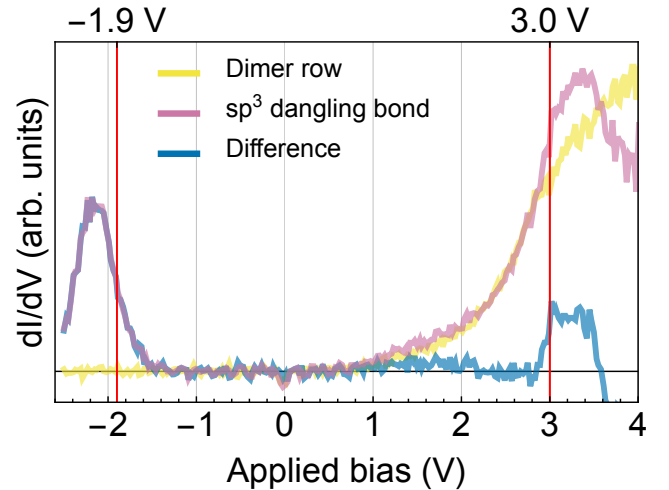
The peaks are broad with a FWHM of approximately 0.5 V (for the peak at negative bias) and 1 V (for the peak at positive bias). This requires interpretation for the voltage onset of tunneling, and ultimately this value will be critical to our analysis. We define this onset as the voltage corresponding to the half maximum for the *difference* between the dI/dV curves between the dangling bond and dimer row. The values for this tunneling onset are indicated in Figure 2 (b) as -1.9 V and $+3.0$ V.

B. Electronic band structure

The electronic band structure of the diamond slab with a single sp^3 dangling bond is presented in Figure 3 (a). The states of interest are those localised to the sp^3 dangling bond near the bulk Fermi level (E_f). For boron-doped diamond, E_f is positioned approximately $+0.2$ eV above the bulk valence band maximum (VBM). The defect-related states have been identified through explicit visualisation of charge densities at the Γ -point obtained using HSE06 functionals (c.f. Figure 1). This reveals four key states relevant to STS which are associated with the defect electronic structure. There are three occupied state positioned at -0.7 eV, -0.55 eV, and -0.2 eV relative to E_f and an unoccupied state located $+2.9$ eV



(a) STM image of the H-C(100):2 \times 1 surface displaying a myriad of defects amongst the characteristic dimer rows. Indicated in green is a single vacancy, in red a CH_2 bridge, and in blue the dangling bond. It is characterised by a bright asymmetric feature.

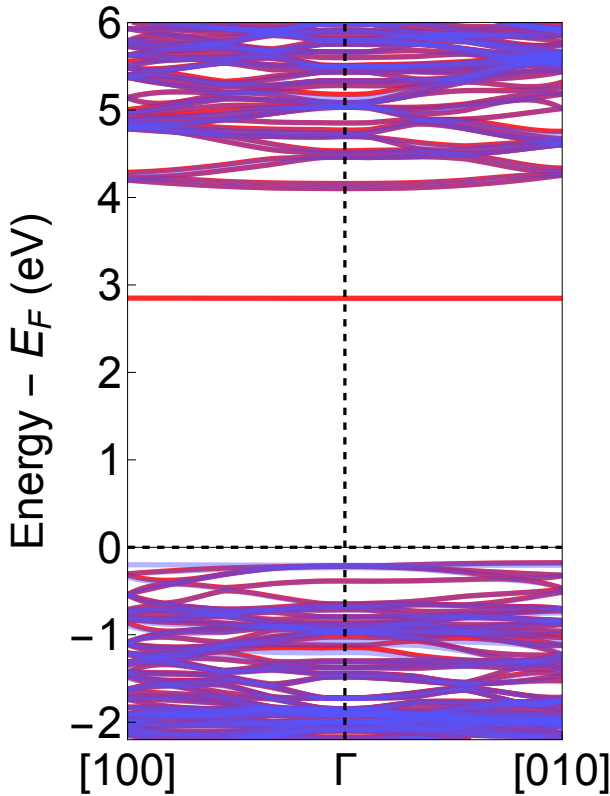


(b) dI/dV spectrum of an sp^3 dangling bond.

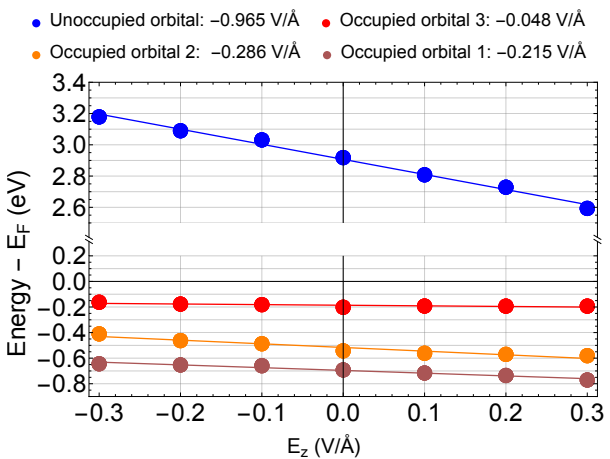
FIG. 2: Experimental spectra of the (100) diamond surface.

above E_f . For reference, the occupied states will be labeled from 1 to 3 in ascending order of energy. It is assumed that the two peaks in the dangling bond STS spectrum can be attributed to tunneling into at least two of these four states.

The diamond surface experiences a considerable electric field during STS. This produces a linear Stark shift in the energy of the defect states which must be accounted for when analysing the STS spectrum. This Stark shift is demonstrated explicitly in Figure 3 (b), which presents



(a) Spin-decomposed band structure. Bands are generated using PBE and the energies shifted based on HSE06 calculations at the Γ -point.



(b) Stark shift of localised sp^3 states at Γ -point.

FIG. 3: One-electron energies for the occupied and unoccupied orbitals corresponding to the sp^3 dangling bond on the H-C(100):2 \times 1 surface.

the energy of the four key defect states as a function of electric field. The charge density of the unoccupied state extends further into the vacuum region than the occupied states, and therefore experiences the greatest Stark shift.

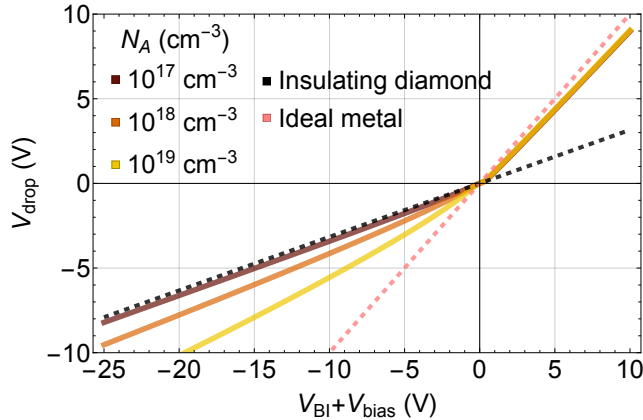
C. Band bending

Application of a bias voltage during STM/STS translates the tip Fermi level relative to the bulk electronic band structure. However, unlike a metallic surface, the electric field produced by the tip is not completely screened at the diamond surface. Due to diamond's wide band gap there is no accumulation of intrinsic charge carriers at the surface. This can be contrasted to the behaviour of an ideal capacitor. In diamond, the applied bias between tip and sample is not fully dropped across the vacuum region. Consequently, for an applied bias V_a , the tip Fermi level is *not* translated by energy qV_a relative to the diamond surface states. Instead, it is translated by a reduced amount qV_d , where $V_d = V_a - V_{bb}$ for V_{bb} the band bending potential at the surface.

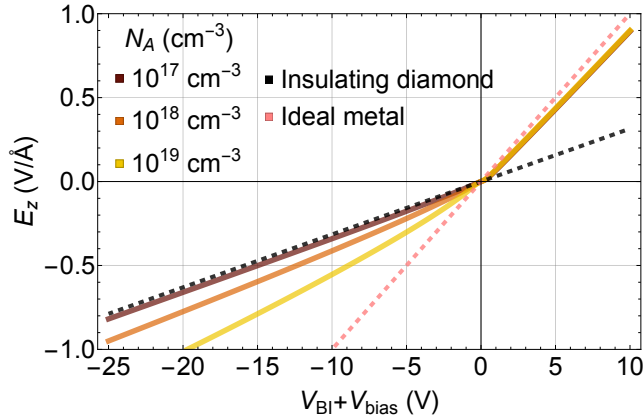
This means that the peak positions in Figure 2 (b) cannot be directly compared to the electronic band structure in Figure 3 (a). One must also account for the band bending produced by the reduced screening response at the diamond surface. This screening is asymmetric depending on the polarity of the bias. At positive sample bias, holes accumulate at the surface and provide a strong screening response. At negative sample bias the screening response is due to ionized boron acceptors, which are deep defects with an activation energy of approximately 0.4 eV. In contrast to shallow dopants in silicon, ionization is incomplete in boron-doped diamond and the screening response is poor. Large negative biases are therefore required to translate the tip Fermi level relative to the defect states.

Fortunately, the voltage drop and surface electric field can be quantified precisely using electrostatic modeling. In our circumstance, this modeling depends on three key variables within Poisson's equation and its boundary conditions: the acceptor concentration (N_A), the absolute tip-surface separation (t_H), and the built-in voltage (V_{BI}). The latter is defined by the difference in work functions between tip and sample, and can be calculated experimentally through measuring the function $I(t_H)$. This is performed in the Supplementary Material and yields a value of -0.9 eV. For our sample we estimate that $10^{16} \text{ cm}^{-3} \leq N_A \leq 10^{20} \text{ cm}^{-3}$. Finally, t_H is generally unknown during STM/STS and difficult to quantify, but is generally within the tunneling regime of 5 – 10 Å. Both N_A and t_H are therefore unknown (but constrained) variables, and the goal of Section IV is to determine them through fitting to the STS spectrum in Figure 2 (b).

The effects of band bending are demonstrated explicitly in Figure 4. We plot the relationship between V_d and the electric field at the surface as a function of V_a and N_A . The accumulation of holes at positive sample bias produces a screening response which is comparable to an ideal metal surface ($V_a = V_d$). However, at negative sample bias the voltage drop is much lower than the applied bias. Peaks at negative bias in the dI/dV spectrum therefore correspond to states which are *higher* in energy within the surface electronic structure. Note that



(a) Voltage drop at the diamond surface.



(b) Electric field at the diamond surface.

FIG. 4: The voltage drop and electric field as a function of applied bias. Due to screening effects produced by holes and ionised acceptors, the tip Fermi level does translate commensurately with the applied bias relative to the band structure of the sample surface.

the screening response reduces with N_A due to a lower density of ionized defects, and increases with t_H due to a greater voltage drop occurring across an extended vacuum region.

IV. DISCUSSION

The defect states contributing to the STS spectrum in Figure 2 (b) can now be elucidated. Firstly, the Stark shifts in Figure 3 (b) describe how the defect state energies are modified due to an applied electric field. Secondly, the electrostatic modeling presented in Figure 4 describes the electric field produced by an applied bias, and how this applied bias translates the tip Fermi level relative to the defect states. Through fitting the unknown variables N_A and t_H , these two results uniquely determine which states produce the experimental peaks at -1.9 eV and 3.0 eV.

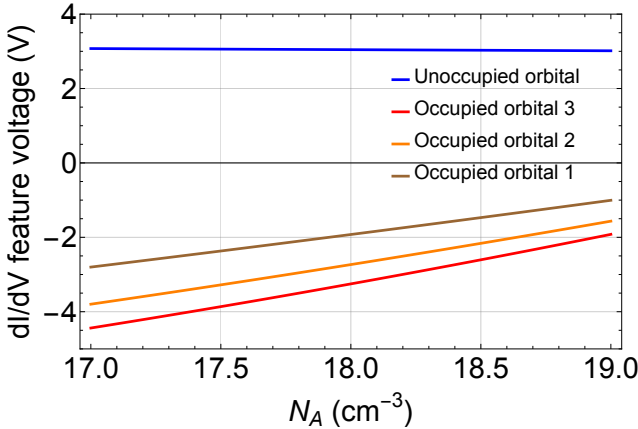
To make this fitting procedure explicit, consider the

variation of peaks in the dI/dV curve as a function of the dependent variables. Figure 5 depicts the theoretical tunneling onset voltage for the four localised states as a function of N_A , t_H , and V_{BI} . The effect of each variable has been considered in isolation by fixing the other two variables to realistic values. Two key results can be inferred from Figure 5. Firstly, the bias required to tunnel into the unoccupied orbital is effectively fixed at 3 V and varies only weakly with N_A , t_H , and V_{BI} . As expected, band bending is minimal due to the effective screening of the mobile holes at positive bias. In contrast, the occupied orbitals experience significant band bending due to the ineffective screening response of the ionised acceptors. Secondly, under many conditions the three occupied orbitals are close together, particularly for $V_{BI} > 0$. However, the experimental spectrum in Figure 2 (b) displays a single peak at negative voltage with FWHM of approximately 0.5 V. Given that we know $V_{BI} = -0.9$ eV, this implies that occupied orbitals 1 and 2 are too low in energy to appear in the STS spectra because they lie below the measured voltage range. Hence, the two peaks in Figure 2 can be associated with tunneling into the unoccupied orbital and occupied orbital 3.

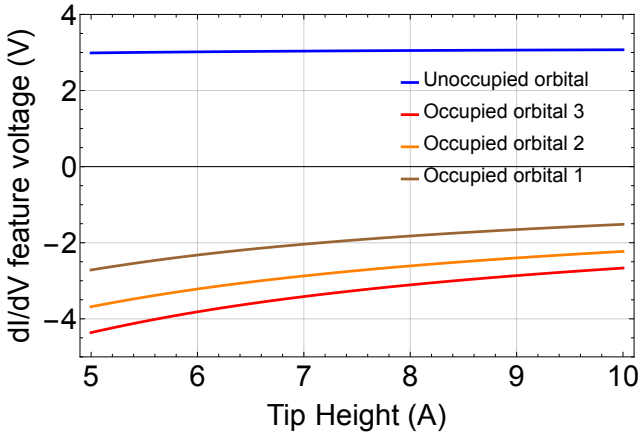
We now fit t_H and N_A based on the voltages required for the onset of tunnelling into occupied orbital 3 and the unoccupied orbital. The positions of these features in the dI/dV spectra depend on both the tip–surface distance and the boron concentration: the negative-bias feature associated with occupied orbital 3 is strongly sensitive to t_H and N_A , whereas the positive-bias feature from the unoccupied orbital is only weakly affected. Given the experimental ambiguity in the exact feature positions, the system is effectively overdetermined; many combinations of t_H and N_A reproduce essentially the same voltages. Taking the tunneling onsets at -1.9 V and 3.0 V as representative yields $t_H = 6.2$ Å and $N_A = 1.3 \times 10^{19}$ cm $^{-3}$. However, a small variation of ± 0.05 V in the unoccupied peak position permits solutions with t_H between 5 Å and 9 Å. Thus, ambiguity in defining the onset of tunneling into the unoccupied orbital directly translates into uncertainty in the absolute tip height. This is ultimately due to the asymmetry in band bending at positive and negative biases.

V. CONCLUSION

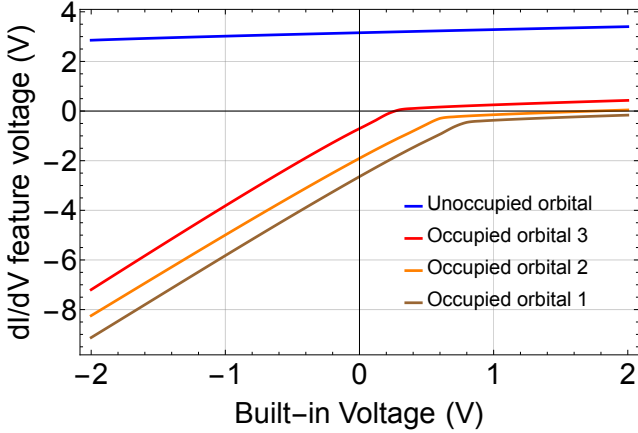
Peak positions in dI/dV curves do not provide a reliable indicator of orbital energies for wide bandgap semiconductors. For boron-doped diamond, band bending decreases the energy of occupied surface states relative to the bulk Fermi level. Electrostatic modeling demonstrates that the extent of this band bending is dependent on three factors: the doping concentration, the tip height, and the built-in voltage. Fortunately, first-principles techniques can calculate the variation in defect energies due to these factors. Given an STS spectrum of a given defect, it is then possible to fit these factors by fitting.



(a) Position of peaks in dI/dV spectra as a function of N_A ($V_{BI} = -0.9$ V, $t_H = 7.5$ Å).



(b) Position of peaks in dI/dV spectra as a function of t_H ($V_{BI} = -0.9$ V, $N_A = 10^{18}$ cm $^{-3}$).



(c) Position of peaks in dI/dV spectra as a function of V_{BI} ($t_H = 7.5$ Å, $N_A = 10^{18}$ cm $^{-3}$).

FIG. 5: Theoretical peak position for each of the four electronic states in the tunneling spectrum.

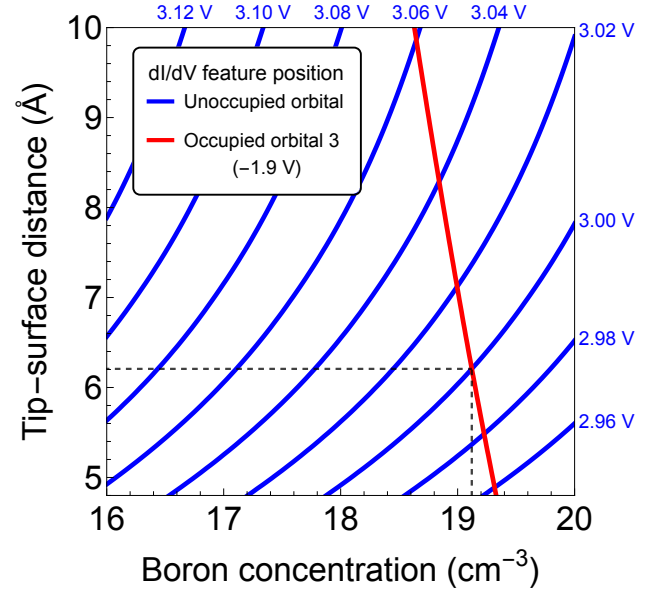


FIG. 6: Contour plot for dI/dV feature positions corresponding to the unoccupied orbital and occupied orbital 3. The negative-bias feature is strongly dependent on both t_H and N_A , whereas the positive-bias feature is only weakly dependent, so many tip-surface distances yield effectively the same N_A . Assigning the occupied and unoccupied features to -1.9 V and 3.0 V gives $t_H = 6.2$ Å and $N_A = 1.3 \times 10^{19}$ cm $^{-3}$, but an uncertainty of ± 0.05 V in the unoccupied peak allows t_H between 5 Å and 9 Å.

This procedure has been implemented for the sp³ dangling bond on H-C(100):2 × 1 to obtain a comprehensive understanding of its STS signature. We identify two key features in the dI/dV curve. Firstly, tunneling onset occurring at +3.0 V which is resistant to the effects of band bending and corresponding to the mid-gap unoccupied orbital. We note that previous work indicates that many other diamond defects also possess unoccupied mid-gap states near 3 eV[3]. Secondly, a peak at negative bias which varies in position with dopant concentration, tip height, and the built-in voltage, corresponding to an occupied orbital near the VBM. The presence of these two states can aid in the identification of the sp³ dangling bond during STM imaging in addition to imaging topography.

REFERENCES

[1] Lachlan M Oberg, Marietta Batzer, Alastair Stacey, and Marcus W Doherty. Nitrogen overgrowth as a catalytic mechanism during diamond chemical vapour deposition. *Carbon*, 178:606–615, 2021.

[2] Alastair Stacey, Nikolai Dotschuk, Jyh Pin Chou, David A. Broadway, Alex K. Schenk, Michael J. Sear, Jean Philippe Tetienne, Alon Hoffman, Steven Prawer, Chris I. Pakes, Anton Tadich, Nathalie P. de Leon, Adam Gali, and Lloyd C.L. Hollenberg. Evidence for primal sp^2 defects at the diamond surface: Candidates for electron trapping and noise sources. *Advanced Materials Interfaces*, 6, 2019.

[3] Yi-Ying Sung, Lachlan Oberg, Rebecca Griffin, Alex K Schenk, Henry Chandler, Santiago Corujeira Gallo, Alastair Stacey, Tetiana Sergeieva, Marcus W Doherty, Cedric Weber, and Christopher I Pakes. Identification of defects and the origins of surface noise on hydrogen-terminated (100) diamond. *Advanced Materials Interfaces*, 12:2400695, 2025.

[4] Jyh-Pin Chou, Péter Udvarhelyi, Nathalie P de Leon, and Adam Gali. Ab initio study of (100) diamond surface spins. *Physical Review Applied*, 20:14040, 7 2023.

[5] L M Oberg, M O de Vries, L Hanlon, K Strazdins, M S J Barson, M W Doherty, and J Wrachtrup. Solution to electric field screening in diamond quantum electrometers. *Phys. Rev. Applied*, 14:14085, 7 2020.

[6] Michael S J Barson, Lachlan M Oberg, Liam P McGuinness, Andrej Denisenko, Neil B Manson, Jörg Wrachtrup, and Marcus W Doherty. Nanoscale vector electric field imaging using a single electron spin. *Nano Letters*, 21:2962–2967, 2021. PMID: 33739842.

[7] M Kim, H Mamin, M Sherwood, K Ohno, D Awschalom, and D Rugar. Decoherence of near-surface nitrogen-vacancy centers due to electric field noise. *Physical Review Letters*, 115:87602, 8 2015.

[8] Marcus Doherty, Lachlan Oberg, Cedric Weber, Tetiana Sergeieva, Chris Pakes, Alex Schenk, and Alastair Stacey. Atomic scale fabrication of diamond quantum computers, 2023.

[9] Lachlan Oberg. *Atom-scale Fabrication and Applications of Diamond Quantum Devices*. PhD thesis, Research School of Physics, ANU College of Science, The Australian National University, 2024.

[10] Lachlan Oberg, Cedric Weber, Hung-Hsiang Yang, Wolfgang M Klesse, Philipp Reinke, Santiago Corujeira Gallo, Alastair Stacey, Christopher I Pakes, and Marcus W Doherty. Bottom-up fabrication of scalable room-temperature diamond quantum computing and sensing technologies. *Materials for Quantum Technology*, 5(3):033001, jul 2025.

[11] Marcus Doherty, Lachlan Oberg, Cedric Weber, Tetiana Sergeieva, Chris Pakes, Alex Schenk, and Alastair Stacey. Atomic scale fabrication of diamond quantum computers, 2025. Published 29 May 2025; application filed 29 November 2022.

[12] K. Bobrov, A. J. Mayne, A. Hoffman, and G. Dujardin. Atomic-scale desorption of hydrogen from hydrogenated diamond surfaces using the stm. *Surface Science*, 528:138–143, 3 2003.

[13] R M Feenstra, Y Dong, M P Semtsiv, and W T Maslinsk. Influence of tip-induced band bending on tunnelling spectra of semiconductor surfaces. *Nanotechnology*, 18:044015, 2007.

[14] R M Feenstra. A prospective: Quantitative scanning tunneling spectroscopy of semiconductor surfaces. *Surface Science*, 603:2841–2844, 2009.

[15] G. Kresse and J. Hafner. Ab initio molecular dynamics for liquid metals. *Physical Review B*, 47:558–561, 1993.

[16] G. Kresse and J. Furthmüller. Efficiency of ab-initio total energy calculations for metals and semiconductors using a plane-wave basis set. *Computational Materials Science*, 6:15–50, 1996.

[17] G. Kresse and J. Furthmüller. Efficient iterative schemes for *ab initio* total-energy calculations using a plane-wave basis set. *Physical Review B*, 54:11169–11186, 1996.

[18] J. P. Perdew, K. Burke, and M. Ernzerhof. Generalized gradient approximation made simple. *Physical Review Letters*, 77:3865–3868, 1996.

[19] J. Heyd, G. E. Scuseria, and M. Ernzerhof. Hybrid functionals based on a screened coulomb potential. *The Journal of Chemical Physics*, 118:8207–8215, 2003.

Supplementary Material:

Tunneling probe-based identification of the sp^3 dangling bond on the H–C(100):2 × 1 surface

S1. BUILT-IN VOLTAGE DETERMINATION

The built-in voltage difference (V_{BI}) may be calculated as the difference between the work function of the sample (Φ_s) and tip (Φ_t) surfaces. The work function of the H–C(100):2 × 1 surface can be determined from its electron affinity ($\chi = -1.3$ eV), bulk band gap ($E_g = 5.5$ eV), and Fermi level ($E_F \approx 0.2$ eV for boron-doped diamond). This yields $\Phi_s = E_g + \chi - E_F \approx 4.0$ eV.

The tip work function cannot be determined in such a straightforward manner, as its atomic composition and therefore electronic structure is unknown. However, it is possible to measure the tip work function explicitly through the function $I(t_H)$ as follows. The assumptions required are similar to that of Chen's approximation for tunneling matrix elements[1]. Namely, the crystal potential from the sample and tip subsystems vanishes within the vacuum region. In this region, the Schrödinger equation for states of the tip apex (ϕ_μ) which are close in energy to the Fermi level reduce to the Helmholtz equation. That is,

$$(\nabla^2 - \kappa^2)\phi_\mu(\mathbf{r}) = 0, \quad (1)$$

where $\kappa = (2m\Phi_t)^{1/2}/\hbar$ and m the electron mass. The solutions to equation (1) decrease exponentially as a function of radial distance from the tip apex. Calculation of the tunneling matrix elements using Bardeen's theory yields the following dependence of current on tip height,

$$I(t_H) \propto \exp(-2\kappa \cdot z).$$

Hence, experimental measurement of $I(t_H)$ can be used to determine κ and therefore Φ_t .

Figure S1 presents a logarithmic plot of $I(t_H)$ sampled above the H–C(100):2 × 1 dimer rows at an applied bias of 1.5 V. It reveals that $\kappa = 0.9 \text{ \AA}^{-1}$ which corresponds to $\Phi_t = 3.1$ eV and $V_{BI} \approx -0.9$ eV. Consequently, at zero applied bias the Fermi level of the two subsystems will be equalised through the migration of holes from sample to tip. The diamond surface states will bend downwards, requiring a lower applied bias to achieve tunneling into the occupied states.

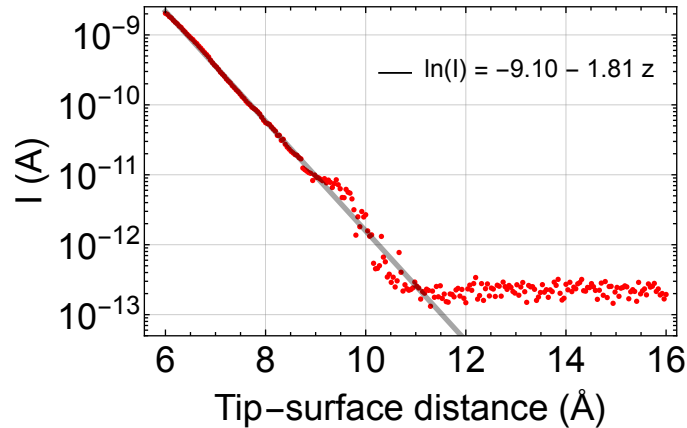


FIG. S1: Logarithmic plot of current vs tip-surface separation distance recorded on the H–C(100):2 × 1 surface at 1.5V using a Ag/W tip. A linear fitting between 6–10 \AA reveals a value of $\kappa = 0.9 \text{ \AA}^{-1}$ and $\Phi_t = 3.1$ eV.

REFERENCES (SUPPLEMENTARY MATERIAL)

[1] C. Julian Chen. Tunneling matrix elements in three-dimensional space: The derivative rule and the sum rule. *Phys. Rev. B*, 42:8841–8857, Nov 1990.